THE JOURNAL OF PHYSICAL CHEMISTRY C

Article

Cite This: J. Phys. Chem. C 2019, 123, 14058−14066

pubs.acs.org/JPCC

Room-Temperature Electron Transport in Self-Assembled Sheets of PbSe Nanocrystals with a Honeycomb Nanogeometry

Maryam Alimoradi Jazi,[†,‡] Aditya Kulkarni,[†,§] Sophia Buhbut Sinai,[‡] Joep L. Peters,[‡] Eva Geschiere,[§] Michele Failla,[§] Christophe Delerue,[∥] Arjan J. Houtepen,[§] Laurens D. A. Siebbeles,[*,§] and Daniel Vanmaekelbergh[*,‡]

[‡]Debye Institute for Nanomaterials Science, University of Utrecht, Princetonplein 1, 3584 CC, Utrecht, The Netherlands

[§]Optoelectronic Materials Section, Department of Chemical Engineering, Delft University of Technology, Van der Maasweg 9, 2629 HZ, Delft, The Netherlands

[∥]IEMN, Department of ISEN, UMR CNRS 8520, 59046 Lille, France

Supporting Information

ABSTRACT: It has been shown recently that atomically coherent superstructures of a nanocrystal monolayer in thickness can be prepared by self-assembly of monodisperse PbSe nanocrystals, followed by oriented attachment. Superstructures with a honeycomb nanogeometry are of special interest, as theory has shown that they are regular 2-D semiconductors, but with the highest valence and lowest conduction bands being Dirac-type, that is, with a linear energy-momentum relation around the K-points in the zone. Experimental validation will require cryogenic measurements on single sheets of these nanocrystal monolayer superstructures. Here, we show that we can incorporate these fragile superstructures into a transistor device with electrolyte gating, control the electron density, and measure the electron transport characteristics at room temperature. The electron mobility is 1.5 ± 0.5 $cm^2\ V^{-1}\ s^{-1}$, similar to the mobility observed with terahertz spectroscopy on freestanding superstructures. The terahertz spectroscopic data point to pronounced carrier scattering on crystallographic imperfections in the superstructure, explaining the limited mobility.

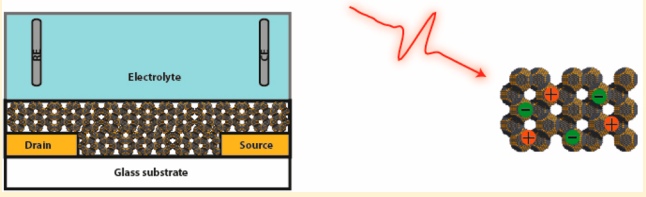

Quantum dot solids composed of colloidal nanocrystals (NCs) have attracted strong interest for about two decades. Such solids show optoelectronic properties that reflect the properties of the individual nanocrystalline quantum dots, together with the dipolar and electronic coupling between them. Since there are many types of NCs that can be incorporated in a solid and the quantum coupling between the NCs can be varied by control over the NC surface chemistry, NC solids form a material platform with considerable tunability and versatility. This platform is of great interest to address basic scientific questions in quantum transport and shows promise for future optoelectronics.[1−12]

In this field, solids that are formed by NC assembly followed by oriented attachment of the NCs constitute a special class, since oriented attachment results in atomically coherent systems and strong quantum coupling. Over the years, atomically coherent one-dimensional rods,[13,14] two-dimensional quantum wells,[15] and nearly three-dimensional[16] nanostructured but atomically coherent systems have been reported. Since, due to the NC/NC epitaxy, the quantum coupling is strong, the energy level and band structure of these systems are determined by their overall dimensions. A remarkable class is 2-D superstructures that show a silicene-type honeycomb structure: these systems retain the semiconductor band gap, but the highest valence and lowest conduction bands show a linear dispersion near the K-points of the Brillouin zone. This would mean that, at sufficiently low temperature and with precise control of the Fermi level at around the K-points, massless electrons (holes) may dominate the transport properties, as in graphene.[17]

However, before this type of physics can be explored, several challenges must be addressed: One must be able to prepare sufficiently large domains of honeycomb superlattices to incorporate them in an electrical device with suitable contacts and to change the Fermi level in a controlled way by gating. Control over the band occupation also means that a decent knowledge on the presence of in-gap states is a prerequisite. Second, it will be required to cool down the entire transistor system (at a given position of the Fermi level) without mechanical or electrical breakage.

Here, we describe the first steps in this field by a room-temperature study of the band occupation and electron transport in silicene-type honeycomb structures prepared from PbSe NCs. We used a transistor device, allowing to measure the electronic properties under electronic equilibrium and terahertz (THz) spectroscopy to measure the transient behavior of photogenerated electrons and holes. This study is motivated by the fact that we recently were able to reproducibly fabricate

Received: April 15, 2019
Published: May 7, 2019

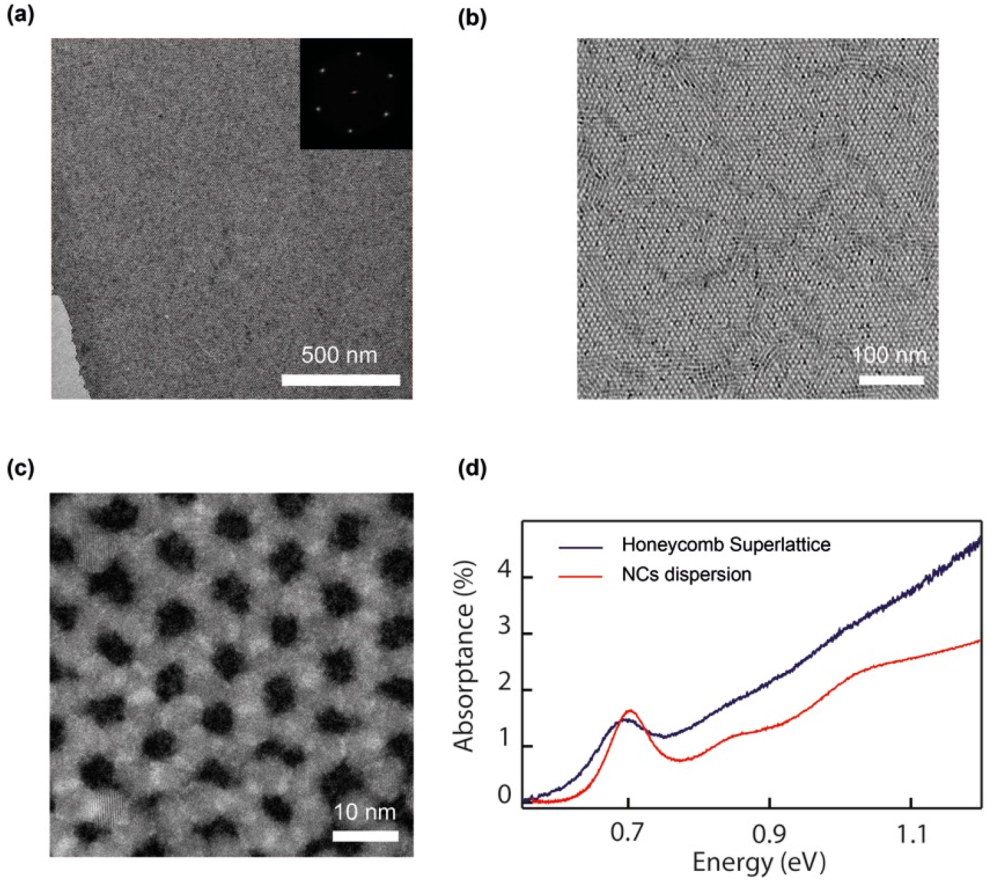

Figure 1. Structural properties of the PbSe honeycomb superlattice studied here: (a) TEM overview of a PbSe superlattice with honeycomb nanogeometry; the inset is the Fourier transform of the image showing that the honeycomb periodicity is long ranged and holds for the entire image. (b) TEM image of a superlattice with smaller honeycomb domains connected by slightly disordered grain boundaries. (c) High resolution HAADF-STEM image showing several types of NC misalignment in the honeycomb structure. (d) Absorption spectrum of a single-layer honeycomb superlattice deposited on a quartz substrate compared to that of dispersed NCs. The first excitonic absorption feature of the PbSe superlattice shows a red shift and broadening, compared to the NCs in dispersion. For the honeycomb superlattice monolayer on a quartz substrate, the absorption is 1.5% at a photon energy of 0.7 eV. The absorption of NC dispersion is scaled down for comparison to the superlattice.

extended (>100 μm) domains of PbSe honeycomb structures by nanocrystal assembly and oriented attachment.[18] We show that we can incorporate wet-chemically prepared superstructures as individual silicene sheets in an electrolyte gated device. We can change the Fermi level in a controlled way and occupy the lowest conduction band with up to four electrons, without interference of midgap electron traps. By moving the Fermi level to lower energies toward the valence band, holes are injected. They might either occupy the valence band or mainly trap states in the gap. The electron mobility measured in the transistor type device (about 1.5 ± 0.5 cm^2 V^{-1} s^{-1}) compares well with that obtained by THz spectroscopy. The frequency-dependent THz results indicate that the room temperature electron mobility is not limited by electron scattering on lattice phonons, but mostly by lattice imperfections.

FORMATION OF 2-D HONEYCOMB SUPERLATTICES OF PbSe

We prepared 2-D honeycomb superlattices from PbSe NCs (with the size of 6.15 ± 0.4 nm) dispersed in toluene by self-assembly at the toluene-nitrogen interface and oriented attachment (see Supporting Information (Figure S1)).[18] An atomically coherent silicene-type honeycomb structure is formed by epitaxial attachment of the PbSe NCs via three of their 6 {100} facets. A part of such a honeycomb structure is shown in Figure 1a. The Fourier transform of the image in the inset shows that the honeycomb periodicity holds for the entire image and is thus long ranged. We remark here that, due to the epitaxial connection, the quantum coupling between the NCs is strong. Atomic tight binding (TB) calculations have shown that this coupling results in mini-band formation with a bandwidth in 0.1 eV range.[19] This means that, for ideal honeycomb structures, high mobility values only limited by phonon scattering are expected. On the other hand, disorder could also limit carrier transport. Several types of disorder have been observed and detailed in a recent work:[18] Nonperfect epitaxial connections between the NCs is probably the most important origin of crystallographic disorder. In the experiments described here, the PbSe superstructures also showed slightly more disordered regions between the honeycomb domains (Figure 1b). Disorder due to the nanocrystal misalignment in the lattice is obvious from Figure 1c.

LIGHT ABSORPTION BY A PbSe HONEYCOMB MONOLAYER

The optical absorption spectrum of the NCs dispersed in tetrachloroethylene exhibits a peak at 0.7 eV related to the first exciton transition (Figure 1d). For a single PbSe honeycomb

DOI: 10.1021/acs.jpcc.9b03549
J. Phys. Chem. C 2019, 123, 14058−14066

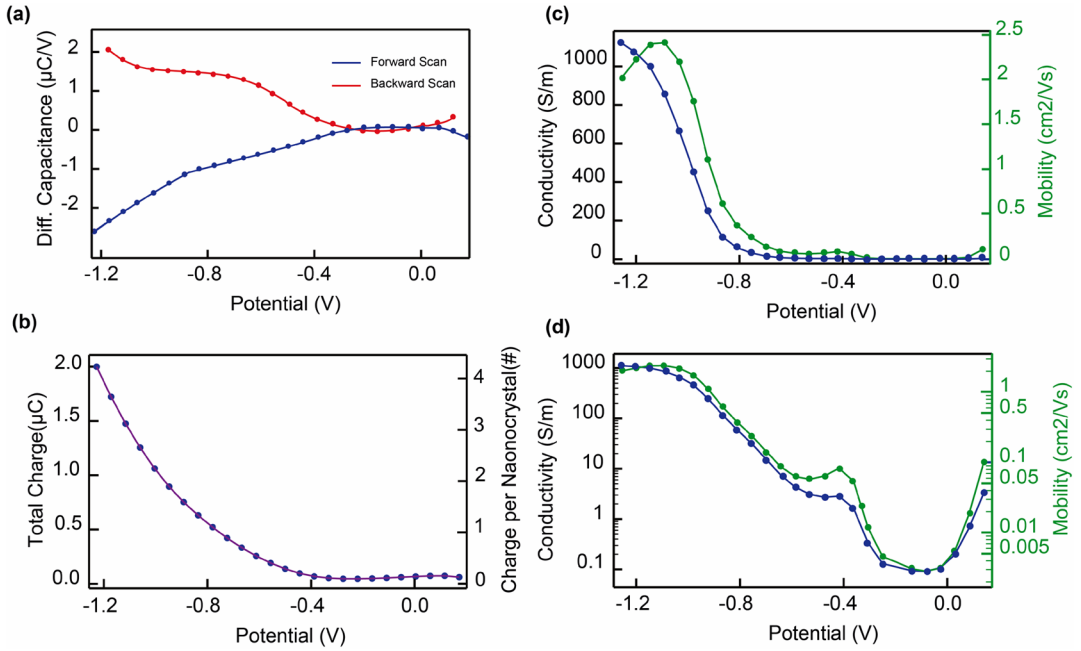

Figure 2. Electron injection and electron transport characteristics in a passivated PbSe honeycomb superstructure incorporated in an electrolyte gated transistor: (a) Differential capacitance of a passivated PbSe honeycomb superlattice measured in forward (from 0.2 to −1.2 V) and backward scan. (b) The total injected charge and the charge per NC site as measured in the forward scan. (c) The conductivity (blue) and the electron mobility (green) of the superlattice obtained from the source-drain conductance (see Figure S5), the geometry of the source-gap-drain fingers system and the charge density presented as a function of the electrochemical potential. (d) The conductivity (blue) and the electron mobility (green) of the superlattice in logarithmic scale.

layer, the first feature is broadened such that it almost looks as a step, and it is also red-shifted. Similar features have been observed for the square superlattices.[20] The broadening is due to quantum coupling between the PbSe NCs, ultimately resulting in band formation (see also below).[3,20,21] The red shift has been attributed to the effect of the dielectric environment.[3,20] The band structure obtained from a TB calculation is presented in Figure S2 without inclusion of many-body electron−hole interaction effects, which are probably weak, due to the large dielectric constant of PbSe. The calculated band structure yields an effective mass of 0.21 m_0 for electrons (m_0 the free electron mass). We should remark here that models for 2-D quantum wells predict a value of the absorptance of 2.3% (related to the fine structure constant) for a single quantum well. The value that we measure is 1.5%, about half the predicted value for a single free-standing layer. A similar reduction of absorption of a 2-D monolayer has been observed previously and was attributed to the presence of the quartz substrate.[22]

TRANSPORT MEASUREMENTS IN AN ELECTROLYTE-GATED TRANSISTOR

Single sheets of a honeycomb superlattice were incorporated into a transistor-type device by horizontal transfer of the structure from the ethylene glycol (EG) surface on which it was formed (see Methods). The surface of the sample is treated by $PbCl_2$, which has been shown to passivate surface traps and improve electronic transport.[23] Using electrochemical gating, the number of conduction electrons in the honeycomb superlattice can be controlled. From the source-drain conductance and the electrode-gap geometry, the electron conductivity and, finally, the electron mobility can be obtained.[20]

In order to investigate the occupation of the bands with electrons (holes), differential capacitance measurements were performed (see Methods). Figure 2a shows the differential capacitance characterizing the injection of electrons and holes into the PbSe honeycomb superlattice treated with $PbCl_2$. It can be seen that electron injection sets on at −0.4 V (vs Ag, reference electrode) and increases gradually up to a sample potential of −1.2 V. The shapes of the forward and backward scans are similar, but not entirely identical. It means that the charge injection is not entirely electrochemically reversible, and some minor side reactions, such as the reduction of residual molecular oxygen, may be ongoing. At positive potentials, the differential capacitance rises, showing that positive charge carriers are injected into the PbSe superstructure.

The total amount of injected charge carriers and the number of carriers per NC site (=1/2 unit cell) in the forward scan are depicted in Figure 2b. The method to determine this number is outlined in the SI, section 4. At the most negative potential (−1.2 V), we observed four electrons per NC site, meaning that the 8-fold degenerate S-type conduction band is, in principle, half occupied. We should mention here that the uncertainty in the occupation number is relatively large due to the uncertainty in the effective active area of the device (see details in SI, section 4). An optical microscope image of the active channel of the device is presented in Figure S4 showing that basically the whole area of the channel is covered by the superlattice. Also note that, at room temperature, electrons can be thermally excited from the S-type mini-band into the P-type mini-band. Strongly charged PbSe NCs have also been reported recently.[24−28]

At sample potentials more negative than −0.5 V, the source-drain transport current increased linearly with the source-drain bias (see Figure S6); the slope provides the conductance of the superlattice. From the conductance and the geometry of the

DOI: 10.1021/acs.jpcc.9b03549
J. Phys. Chem. C 2019, 123, 14058−14066

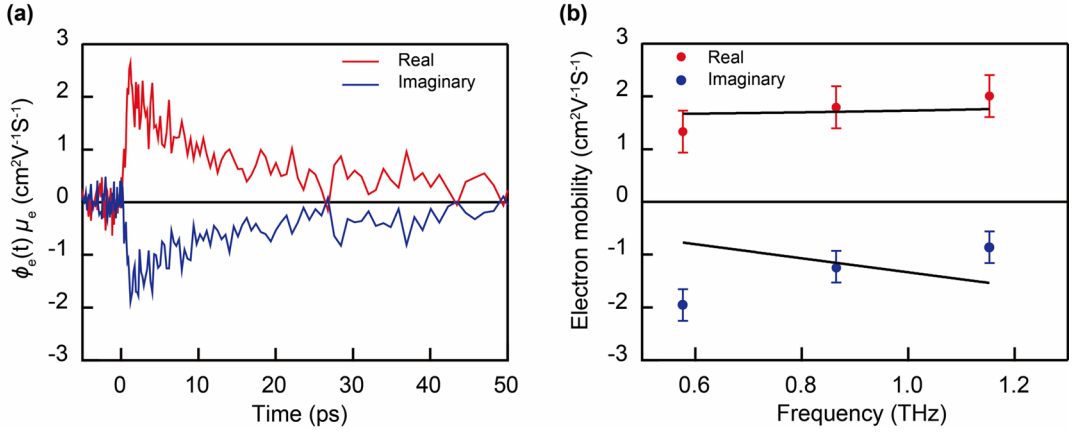

Figure 3. Terahertz photoconductivity obtained by photoexciting the PbSe honeycomb superstructure treated with $PbCl_2$ at photon energy of 1.55 eV. (a) Real (positive signal) and imaginary part (negative signal) of the quantum yield weighted mobility as a function of time obtained at excitation density 2.5×10^{13} cm^{-2}, which corresponds to 10 electron−hole pairs per NC. (b) Experimental frequency-dependent charge carrier mobility (markers) together with fit of the Drude-Smith model to the data.

interdigitated source-drain electrodes and gap, the electronic conductivity was calculated. We have plotted the conductivity of the sample as a function of the sample potential on a linear scale (Figure 2c) and a logarithmic scale (Figure 2d) for convenience. As can be observed in Figure 2c, the conductivity sets on at around −0.5 V and rises steeply with the electrochemical potential, up to 1100 S/m at the most negative potential. For positive electrochemical potentials the differential capacitance increases again, this is accompanied by a small increase of the source-drain conductance (Figure 2d). It appears that the conductivity at positive potential is much smaller than the electron conductivity. This indicates that the injected positive charges to the superlattice might either occupy the valence band, or could occupy localized in-gap states. In the logarithmic scale in Figure 2d, the conductivity shows a step-like peak (not clearly visible on a linear scale) at a potential of −0.4 V. However, the charge density at this potential has a very small value. Therefore, we cannot conclude whether this peak is real and related to the band occupation of the superlattice.

Results obtained with other samples, also a sample that is nontreated with $PbCl_2$, are provided in the SI, section 6. Similar results are obtained for those samples, that is, the onset of the conductivity close to the onset of electron injection, the number of electrons in the conduction band varying between 4 and 8 per nanocrystal site, and a smaller conductance at positive potentials at which holes either occupy the valence band or trap states.

The electron mobility of the sample of Figure 2 calculated from the electron density and conductivity reached a maximum value of 2.3 cm^2 V^{-1} s^{-1} at −1 V. We performed differential capacitance and conductivity measurement on three other PbSe honeycomb devices. On average, we find an electron mobility of 1.5 ± 0.5 cm^2 V^{-1} s^{-1} in the PbSe honeycomb superlattices in the potential window of $-1.05 < V < -0.75$. For the sample nontreated with $PbCl_2$ the mobility was found to have a lower value of 0.4 cm^2 V^{-1} S^{1-} (see Figure S7), which we attribute to the presence of trapping sites that have a negative effect on electron transport.

We further note that at the most negative potentials the conductivity is probably limited somewhat by the contact resistance between the honeycomb superlattice and the gold source and drain contacts. This may explain why the conductivity levels off and why the derived value of the mobility even decreases. Hence, the values obtained here are a lower limit to the intrinsic dc mobility.

TERAHERTZ PHOTOCONDUCTIVITY SPECTROSCOPY

The THz photoconductivity was studied by photoexciting PbSe honeycomb superstructures with 50 fs laser pulses at a photon energy of 1.55 eV. The experimental procedure involves detection of charges and excitons with a single-cycle THz field and is identical to that described previously.[29,30] In general, photoexcitation of a semiconductor leads to formation of free mobile charges that can coexist with bound e−h pairs in the form of neutral excitons.[31−33] Free mobile charges and neutral excitons both contribute to the THz conductivity to an extent that is different for the real and imaginary parts.[34,35] At higher photoexcitation density recombination of free charges into excitons is more likely and, consequently, the quantum yield of charges decreases. If excitons coexist with free charges in the honeycomb superlattice, the relative magnitude of the real and imaginary THz conductivity should depend on the initial photoexcitation density and the decay kinetics of the real and imaginary parts should be different. Since the normalized decay of the real and imaginary parts are identical (see Figure S9) it can be inferred that the contribution of excitons is negligible and the initial quantum yield of charges can be taken equal to 1. The real part (positive sign) of the THz conductivity is due to the in-phase charge velocity in the probing THz field, and the imaginary part (negative sign) is due to the out-of-phase charge velocity.[36−38] The electrolyte gated transistor measurements have shown that holes might mostly occupy localized in-gap states. Therefore, the mobility of holes can be neglected and the THz conductivity can be ascribed to electrons only.

Figure 3 shows the THz conductivity for a PbSe honeycomb superstructure treated with $PbCl_2$ to passivate surface traps. The product of the time-dependent quantum yield of electrons and their mobility: defined $S(t) = \phi_e(t)\mu_e$, with the initial quantum yield $\phi_e(t = 0) = 1$, as discussed above is shown for an excitation density of 2.5×10^{13} cm^{-2}, which corresponds to 10 electron−hole (e−h) pairs per nanocrystal (see Methods). The signal $S(t)$ reaches a maximum value of 2.1 ± 0.4 cm^2 V^{-1} s^{-1} at a pump−probe delay time of 1.5 ps, which reflects the pulse duration of the probing single-cycle THz field. This value of $S(t)$ is

DOI: 10.1021/acs.jpcc.9b03549
J. Phys. Chem. C 2019, 123, 14058−14066

attributed to relaxed charge carriers at the band edge, since for a photoexcitation energy of 1.55 eV initially hot e−h pairs in PbSe NCs cool down to the band edge within a picosecond.[39,40] The electrons are seen to decay via trapping or recombination with a lifetime for half decay of ∼10 ps. Similar results were obtained for lower (0.8×10^{13} cm^{-2}) and higher (2.5×10^{13} cm^{-2}) excitation densities (see Figure S8), which implies that higher-order recombination is not important for these densities.

A comparison of $S(t)$ for the PbSe superstructure passivated with $PbCl_2$ and a nontreated superstructure is shown in Figure S11 for similar excitation densities. It can be clearly seen that surface passivation with $PbCl_2$ enhances the mobility by a factor of four, which is in the same direction to that obtained from the DC device measurements described above. The excitation density of 4.3×10^{13} cm^{-2} needed to observe the THz conductivity in the nontreated superstructure is higher than that used for the structure treated with $PbCl_2$. The higher density leads to a faster decay via recombination and, consequently, a smaller value of $S(t)$, even on short time scales.

To understand the charge transport mechanism, we plot in Figure 3b the frequency-dependent electron mobility obtained by averaging $S(t)$ over a pump−probe delay time interval of 2−6 ps. The increase of the mobility in Figure 3b with frequency ω and the negative imaginary mobility disagree with the simple Drude model.[36] The THz mobility is described by the Drude-Smith model, yielding[41]

$$\mu(\omega) = \frac{e\tau}{m^*(1 - i\omega\tau)}\left(1 + \frac{c}{1 - i\omega\tau}\right) \quad (1)$$

with e representing the elementary charge, τ represents the scattering time, m^* is the effective mass, and $c = \langle \cos\theta \rangle$ is the persistence of velocity parameter accounting for elastic back-scattering, with θ as the scattering angle.

Solving for the real and imaginary parts of the Drude-Smith model yields

$$\mu_{\text{real}}(\omega) = \frac{e\tau}{m^*(1 + \omega^2\tau^2)}\left(1 + \frac{c(1 - \omega^2\tau^2)}{1 + \omega^2\tau^2}\right) \quad (2)$$

$$\mu_{\text{imag}}(\omega) = \frac{e\omega\tau^2}{m^*(1 + \omega^2\tau^2)}\left(1 + \frac{2c}{1 + \omega^2\tau^2}\right) \quad (3)$$

Taking the value of $m^* = 0.21m_0$, from atomistic tight binding (see Figure 4), and fitting expressions 2 and 3 to the frequency-dependent mobility in Figure 3b yields $\tau = 5.2 \pm 0.6$ fs and $c = -0.96 \pm 0.01$. At lower excitation densities we obtain similar values for τ and c (see Figure S9), which indicates that for the densities studied band filling does not affect the THz mobility. The backscattering parameter c close to −1 implies significant backscattering of the charges, which is typical for NC solids.[42,43] The DC mobility obtained from the Drude-Smith fit parameters is 1.7 cm^2 V^{-1} s^{-1}, which is close to the value of 1.5 ± 0.5 cm^2 V^{-1} s^{-1} obtained from the transistor measurements described above. Hence, although the coupling between the NCs in the honeycomb structure is considerable, the electron mobility is strongly limited by scattering at imperfections.

The Drude-Smith fit reproduces the measured real part of the THz mobility, while it does not agree very well with the measured imaginary part. Structural disorder may cause the site-energy of a charge to vary on going from one NC to another. The disorder in the site-energies is roughly equal to the width of the first optical absorption peak of the NCs, which is about 0.1 eV, see Figure 1d. Such disorder is not included in the Drude-Smith model, which may cause the model to be inaccurate for the current material. A more detailed model of charge transport should include effects of disorder, however, that is beyond the scope of this study.

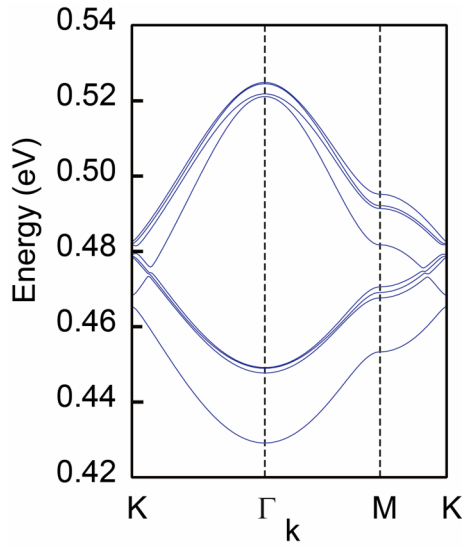

Figure 4. Tight binding (TB) of PbSe honeycomb superlattice. The lowest conduction bands calculated with atomistic tight-binding (TB) theory. The lowest conduction band is 8-fold degenerate (including spin); the degeneration is slightly broken due to quantum coupling of the 4 L points in the zone. The bands show a conventional parabolic dispersion at the Γ-point and a linear Dirac-type dispersion at the K-points. The calculated band structure yields an effective mass of $0.21m_0$ for electrons (m_0 is the free electron mass).

DISCUSSION

We have studied electron transport in single sheets of PbSe with a silicene-type honeycomb geometry. In an ideal case, these structures are atomically coherent: the ⟨111⟩ axis of PbSe rock salt is perpendicular to the plane of the sheet. Each nanocrystal unit is epitaxially connected to three other ones, forming [100]/[100] connections. Silicene honeycomb structures of PbSe, very similar to the ones used here, have been structurally characterized in detail in a recent work.[18] It has been shown that, while the honeycomb domains are very large (>10 μm), there are several types of crystallographic defects, mostly related to nonideal [100]/[100] connections between the constituting NCs. Our electrolyte-gated transport measurements show that the injected electrons occupy the lowest conduction band. However, the injected holes might either occupy the valence band or localized in-gap states. The similarity between the mobility obtained with an electrochemically gated transistor type device and the THz mobility is remarkable (both values are about 1.5 cm^2 V^{-1} s^{-1}). This indicates that the quantum yield for charge carrier photogeneration in the terahertz experiments is close to unity and also that mainly electrons contribute to the THz conductivity. From the above, it is thus reasonable to state that the electron mobility at room temperature is close to 1.5 cm^2 V^{-1} s^{-1} and independent of frequency up to the THz range. The frequency independence implies that charge transport over tens of microns in the transistor measurements (see Figure S3) is as efficient as along the distance (L) probed at THz frequencies, which is the diffusion length during a period (t_{osc}) of the THz field; that is, $L = \sqrt{\frac{4\mu_{\text{dc}} k_B T t_{\text{osc}}}{e}} \sim 5$ nm with k_B being the

DOI: 10.1021/acs.jpcc.9b03549
J. Phys. Chem. C 2019, 123, 14058−14066

Boltzmann constant and T is the temperature. The value of L estimated in this way corresponds to the center-to-center distance between adjacent NCs. Hence, there is a strong electronic coupling between every two NCs, but also a high density of structural defects. First of all, Figure 1b shows that the 2-D domains are about 50−150 nm in size, which means that the electrons see many grain boundaries in their journey between the source and the drain. Second, particularly the THz spectroscopy points to strong scattering. We believe that several type of imperfections, such as nm-crystallographic connection between the nanocrystals and slight misorientations, can cause this intense electron scattering.

Here we provide an interpretation of this result, using the band structure calculated for a PbSe silicene-type honeycomb structure with the same size of the honeycomb units (NCs) and periodicity. The lowest conduction bands calculated with atomistic tight-binding theory are shown in Figure 4. The lowest conduction band is 8-fold degenerate (including spin). It shows a conventional parabolic dispersion at the Γ-point, and a linear Dirac-type dispersion at the K-points. When electrons are injected and the occupation is low, the (low-T) occupation is at the Γ-point. The effective mass of electrons, obtained from atomistic tight binding calculations is $0.21m_0$ (see Figure 4). It is instructive to compare the mobility observed in the honeycomb superstructures with that reported for bulk PbSe. The experimental value for macroscopic crystals of PbSe at room temperature is 1000 $cm^2\ V^{-1}\ s^{-1}$.[44] When we assume that the effective mass in bulk PbSe is $0.1m_0$,[45] the scattering time in a macroscopic PbSe crystal is calculated to be 60 fs, which is more than 10× larger the value of 5.2 ± 0.6 fs we found for the honeycomb superlattice. For the PbSe superstructures, we find that the mobility is almost 500× smaller than the bulk value, whereas the effective mass is only (here at the Γ-point) 2× larger. This means that in our PbSe honeycomb superlattice the electron scattering time is considerably shorter than in the bulk PbSe; hence electrons do not only scatter at lattice phonons, but also at lattice imperfections. This is corroborated by the frequency dependence of the THz mobility. The real and imaginary parts cannot be described by the Drude model, which accounts only for electron−phonon scattering, but back-scattering of electrons on defects needed to be included. The THz mobility could be reproduced approximately by the Drude-Smith model with $c = -0.96 \pm 0.01$, which implies strong backscattering of electrons at imperfections in the PbSe honeycomb superstructures. We believe that imperfect [100]/[100] connections between the NCs are the most important origin of disorder in the PbSe honeycomb superstructures.

Several previous studies have yielded charge mobilities in PbSe NC solids in the range of 1−15 $cm^2\ V^{-1}\ s^{1}$.[6,7,10,23,29,46−48] In these studies of three-dimensional assemblies, the NCs were coupled by small organic linker molecules, and in some cases, the NC solids were thermally annealed or infilled with a metaloxide by atomic layer deposition. Apparently these treatments lead to somewhat high mobilities.[3,48] However, in the present case, please notice that our system is truly 2-D, which increases the relative surface area, and related to this, the density of surface trap states, and also increases the effect of the inhomogeneous electrostatic potential. All these features have a negative effect on electron mobility.

SUMMARY AND OUTLOOK

We studied the electronic properties of PbSe honeycomb superstructures in a transistor-type device and with THz spectroscopy. The results show that electrons occupy the lowest conduction band. The electron mobility is limited by lattice imperfections. The electronic characterization at room temperature presented here shows that it should be possible to subtly move the Fermi level through the energy range of the conduction mini-band. Once PbSe honeycomb transistor-type devices can be cooled down to cryogenic temperatures (i.e., $k_BT \ll$ bandwidth), it should be possible to study the transport physics with the Fermi-level positioned in a narrow energy window, for example, to distinguish the Γ point from K-points. Eventually, this research would enable to display the Dirac character of the carriers in the energy region around the K-points, as has been predicted by simple and advanced theories.

METHODS

Chemicals. Lead acetate trihydrate (99.99%, Sigma-Aldrich), oleic acid (90%, Sigma-Aldrich), 1-octadecene (90%, Sigma-Aldrich), selenium powder (99.99%, Alfa Aesar), trioctylphosphine (90%, Sigma-Aldrich), diphenylphospine (98%, Sigma-Aldrich), 1-butanol (99.8% anhydrous, Sigma-Aldrich), methanol (99.8% anhydrous, Sigma-Aldrich), toluene (99.8% anhydrous, Sigma-Aldrich), ethylene glycol (99.8%,anhydrous, Sigma-Aldrich), acetonitrile (99.8%, anhydrous, Sigma-Aldrich), lithium perchlorate (99.99%, Sigma-Aldrich), and lead(II) chloride (99.99%, Sigma-Aldrich).

PbSe NCs Synthesis. PbSe QDs were synthesized based on the methodology of Steckel et al. method.[49] For the lead precursor, a mixture of 4.77 g of lead acetate, 10.35 g of oleic acid, and 39.75 g of 1-octadecene was heated at 120 °C under vacuum for 5 h. For the selenium precursor, a mixture of 3.52 g of selenium powder, 46.59 mL of trioctylphosphine, and 0.41 mL of diphenylphospine were prepared by dissolving selenium. Subsequently, 10.25 mL of the lead containing solution was heated up to 180 °C and 7.5 mL of the selenium precursor was injected. The mixture was kept at 150 °C for 70 s and the NC growth was quenched with 30 mL of a methanol/butanol mixture (1:2). The NC product solution was centrifuged and the NCs were dissolved in toluene. This concentrated suspension of PbSe NCs was washed twice more with methanol and the NCs were dissolved in toluene.

Formation of Honeycomb Superstructure by Means of Oriented Attachment. Honeycomb superlattices were obtained by the NCs assembly at the toluene-nitrogen interface followed by oriented attachment. We followed an ultraslow procedure that has been developed recently in our group (Figure S1). A small Petri dish was filled with ethylene glycol as a liquid substrate. This dish was placed in a bigger Petri dish that also contained toluene. A certain volume of PbSe NC dispersion in toluene was drop casted on top of ethylene glycol. A beaker was placed on top of the Petri dishes to slow down the toluene evaporation. The evaporation of the toluene solvent and the superlattice formation was really slow and took around 16 h. The honeycomb monolayer was transferred onto a TEM grid for structural characterization, quartz substrates for THz measurement and a device with microstructured gold electrodes, that is, source and drain, separated by a gap for electrolyte gating and transport measurements (details in SI, section 3). The formation of PbSe honeycomb superlattices and their transport to a TEM grid, the quartz substrate and a transport device were performed in a glovebox.

Surface Treatment by $PbCl_2$. In an attempt to passivate the surface traps, the surface of the honeycomb superlattices was treated by $PbCl_2$. For this purpose, a saturated dilution of $PbCl_2$

DOI: 10.1021/acs.jpcc.9b03549
J. Phys. Chem. C 2019, 123, 14058−14066

in methanol was prepared. The substrates with the superlattices were immersed shortly into the $PbCl_2$ dilution and then into methanol, to remove the residuals.

Electron Injection and Transport Measurement in an Electrolyte-Gated Transistor. Electrochemical gating is a well-stablished methods used to investigate the transport properties of 2-D superlattices. The device used for this measurement consists of interdigitated source and drain electrodes, on top of a SiO_2 substrate (details in SI). In this experiment we used acetonitrile containing a Li^+ salt as an electrolyte. An Ag wire and a Pt sheet were inserted into the electrolyte for reference and counter electrodes, respectively. The Fermi level of the superlattices moved toward the conduction band (valence band) by applying negative (positive) potential with respect to the reference electrode by using a potentiostat. To investigate the charge injection into the honeycomb superlattice, differential capacitance measurements were performed. By applying the potential in small steps of 55 mV, the current in an interval time was measured. The integration of the current gave us the total amount of charge injected to the structure. For measurement of the sample conductance at a given potential, a small potential was applied between source and drain electrodes and the source-drain current was measured. As soon as the Fermi level was in the conduction band, the source-drain resistance was Ohmic. The conductivity was obtained from the measured conductance the geometry of the electrodes. Eventually, the electron mobility was obtained from the conductivity and the electron density (details in SI).

Terahertz Conductivity Measurements. The honeycomb superlattice was photoexcited by optical pulses with photon energy 1.55 eV. The photoconductivity was probed by single-cycle THz pulses analogous to our previous work.[29,30] To prevent air exposure, we placed the sample in an airtight sample holder during the photoconductivity measurements. According to the thin film approximation the complex conductivity ($\Delta\sigma(\omega,t)$) of charges averaged over the sample thickness (L) is related to the differential THz signal ($\Delta E(\omega,t)$) via[37,38]

$$\frac{\Delta E(\omega, t)}{E_0(\omega)} = \frac{L\Delta\sigma(\omega, t)}{(1 + n_s)c\varepsilon_0} \tag{4}$$

with e the elementary charge, c the speed of light in vacuum, ε_0 the relative permittivity of free space, and n_s the refractive index of the quartz substrate.

The complex conductivity of charges is related to the quantum yield weighted complex mobility ($\phi_e(t)\mu_e + \phi_h(t)\mu_h$) via[37,38]

$$\phi_e(t)\mu_e + \phi_h(t)\mu_h = \frac{L\Delta\sigma(\omega, t)}{eN_a} \tag{5}$$

with N_a being the number of absorbed photons per unit area (excitation density). Substituting eq 2 into eq 1 and rearranging yields

$$S(t) = \phi_e(t)\mu_e + \phi_h(t)\mu_h = \frac{\Delta E(\omega, t)}{E_0(\omega)}\frac{(1 + n_s)c\varepsilon_0}{eN_a} \tag{6}$$

which is independent of the sample thickness L.

The initial number of e−h pairs per NC was obtained as the ratio of the excitation density and the number of NCs per unit area, with the latter determined to be 2.6×10^{12} NCs per cm^2 from analysis of a TEM image of the honeycomb superlattice.

■ ASSOCIATED CONTENT

Supporting Information

The Supporting Information is available free of charge on the ACS Publications website at DOI: 10.1021/acs.jpcc.9b03549.

Oriented attachment. Electrode design of electrochemical gating measurement. Tight binding calculation of the honeycomb band gap. Conductivity and mobility calculation. Electrochemical measurement on nontreated sample. Normalized real and imaginary part of the THz conductivity at different excitation densities. Drude-Smith model fits to the frequency-dependent electron mobility (PDF)

■ AUTHOR INFORMATION

Corresponding Authors

*E-mail: d.vanmaekelbergh@uu.nl.
*E-mail: l.d.a.siebbeles@tudelft.nl.

ORCID

Aditya Kulkarni: 0000-0002-5840-8768
Joep L. Peters: 0000-0002-3415-648X
Christophe Delerue: 0000-0002-0427-3001
Arjan J. Houtepen: 0000-0001-8328-443X
Laurens D. A. Siebbeles: 0000-0002-4812-7495
Daniel Vanmaekelbergh: 0000-0002-3535-8366

Author Contributions

†M.A.J. and A.K. contributed equally to this work.

Author Contributions

M.A.J., S.B.S., and J.L.P. synthesized and structurally characterized the samples. M.A.J performed electrochemical gating measurements. A.K., E.G., and M.F. performed terahertz photoconductivity spectroscopy measurements. M.A.J., A.K., A.J.H, L.D.A.S., and D.V. analyzed the experimental results. C.D. provided theoretical support. D.V. and L.D.A.S. supervised the work. All the authors discussed the results and contributed to the writing of the manuscript.

Notes

The authors declare no competing financial interest.

■ ACKNOWLEDGMENTS

M.A.J. acknowledges the H2020-MSCA-ITN-2014 Program"-Phonsi, (Nanophotonics by nanocrystals, from integration to single photon operation)" for financial support. A.K. acknowledges the Dutch FOM programme "Designing Dirac carriers in honeycomb semiconductor superlattices" (No. 67595) for financial support. D.V. acknowledges support by ERC research council, ERC-Advanced Grant "First step" (No. 692691). A.J.H. acknowledges support from the European Research Council Horizon 2020 ERC Grant Agreement No. 678004 (Doping on Demand).

■ REFERENCES

(1) Talapin, D. V.; Murray, C. B. PbSe Nanocrystal Solids for n-and p-Channel Thin Film Field-Effect Transistors. *Science* **2005**, *310* (86), 86−90.

(2) Vanmaekelbergh, D.; Liljeroth, P. Electron-conducting quantum dot solids: Novel materials based on colloidal semiconductor nanocrystals. *Chem. Soc. Rev.* **2005**, *34* (4), 299.

(3) Sandeep, C. S. S.; Azpiroz, J. M.; Evers, W. H.; Boehme, S. C.; Moreels, I.; Kinge, S.; Siebbeles, L. D. A.; Infante, I.; Houtepen, A. J. Epitaxially connected PbSe quantum-dot films: Controlled neck

DOI: 10.1021/acs.jpcc.9b03549
J. Phys. Chem. C 2019, 123, 14058−14066

formation and optoelectronic properties. *ACS Nano* **2014**, *8* (11), 11499−11511.
(4) Talapin, D. V.; Lee, J.-S.; Kovalenko, M. V.; Shevchenko, E. V. Prospects of Colloidal Nanocrystals for Electronic and Optoelectronic Applications. *Chem. Rev.* **2010**, *110* (1), 389−458.
(5) Law, M.; Luther, J. M.; Song, Q.; Hughes, B. K.; Perkins, C. L.; Nozik, A. J. Structural, optical, and electrical properties of PbSe nanocrystal solids treated thermally or with simple amines. *J. Am. Chem. Soc.* **2008**, *130* (18), 5974−5985.
(6) Oh, S. J.; Wang, Z.; Berry, N. E.; Choi, J. H.; Zhao, T.; Gaulding, E. A.; Paik, T.; Lai, Y.; Murray, C. B.; Kagan, C. R. Engineering charge injection and charge transport for high performance PbSe nanocrystal thin film devices and circuits. *Nano Lett.* **2014**, *14* (11), 6210−6216.
(7) Oh, S. J.; Berry, N. E.; Choi, J. H.; Gaulding, E. A.; Paik, T.; Hong, S. H.; Murray, C. B.; Kagan, C. R. Stoichiometric control of lead chalcogenide nanocrystal solids to enhance their electronic and optoelectronic device performance. *ACS Nano* **2013**, *7* (3), 2413−2421.
(8) Chiu, S.-C.; Jhang, J.-S.; Chen, J. F.; Fang, J.; Jian, W.-B. Effects of cross-sectional area on the tunneling-junction array in octahedral PbSe colloidal-nanocrystal solids. *Phys. Chem. Chem. Phys.* **2013**, *15* (38), 16127−16131.
(9) Luther, J. M.; Law, M.; Beard, M. C.; Song, Q.; Reese, M. O.; Ellingson, R. J.; Nozik, A. 001-Schottky solar cells based on colloidal nanocrystal films. *Nano Lett.* **2008**, *8* (10), 3488−3492.
(10) Gao, Y.; Aerts, M.; Sandeep, C. S. S.; Talgorn, E.; Savenije, T. J.; Kinge, S.; Siebbeles, L. D. A.; Houtepen, A. J. Photoconductivity of PbSe quantum-dot solids: Dependence on ligand anchor group and length. *ACS Nano* **2012**, *6* (11), 9606−9614.
(11) Kang, M. S.; Lee, J.; Norris, D. J.; Frisbie, C. D. High carrier densities achieved at low voltages in ambipolar PbSe nanocrystal thin-film transistors. *Nano Lett.* **2009**, *9* (11), 3848−3852.
(12) Baumgardner, W. J.; Whitham, K.; Hanrath, T. Confined-but-connected quantum solids via controlled ligand displacement. *Nano Lett.* **2013**, *13* (7), 3225−3231.
(13) Koh, W. K.; Bartnik, A. C.; Wise, F. W.; Murray, C. B. Synthesis of monodisperse PbSe nanorods: A case for oriented attachment. *J. Am. Chem. Soc.* **2010**, *132* (11), 3909−3913.
(14) Cho, K. S.; Talapin, D. V.; Gaschler, W.; Murray, C. B. Designing PbSe nanowires and nanorings through oriented attachment of nanoparticles. *J. Am. Chem. Soc.* **2005**, *127* (19), 7140−7147.
(15) Schliehe, C.; Juarez, B. H.; Pelletier, M.; Jander, S.; Greshnykh, D.; Nagel, M.; Meyer, A.; Foerster, S.; Kornowski, A.; Klinke, C.; et al. Ultrathin PbS sheets by two-dimensional oriented attachment. *Science* **2010**, *329* (5991), 550−553.
(16) Whitham, K.; Hanrath, T. Formation of Epitaxially Connected Quantum Dot Solids: Nucleation and Coherent Phase Transition. *J. Phys. Chem. Lett.* **2017**, *8* (12), 2623−2628.
(17) Castro Neto, A. H.; Guinea, F.; Peres, N. M. R.; Novoselov, K. S.; Geim, A. K. The electronic properties of graphene. *Rev. Mod. Phys.* **2009**, *81* (1), 109−162.
(18) Peters, J. L.; Altantzis, T.; Lobato, I.; Jazi, M. A.; Van Overbeek, C.; Bals, S.; Vanmaekelbergh, D.; Sinai, S. B. Mono- and multilayer silicene-type honeycomb lattices by oriented attachment of PbSe nanocrystals: synthesis, structural characterization, and analysis of the disorder. *Chem. Mater.* **2018**, *30* (14), 4831−4837.
(19) Kalesaki, E.; Delerue, C.; Morais Smith, C.; Beugeling, W.; Allan, G.; Vanmaekelbergh, D. Dirac cones, topological edge states, and nontrivial flat bands in two-dimensional semiconductors with a honeycomb nanogeometry. *Phys. Rev. X* **2014**, *4* (1), 1−12.
(20) Alimoradi Jazi, M.; Janssen, V. A. E. C.; Evers, W. H.; Tadjine, A.; Delerue, C.; Siebbeles, L. D. A.; Van Der Zant, H. S. J.; Houtepen, A. J.; Vanmaekelbergh, D. Transport Properties of a Two-Dimensional PbSe Square Superstructure in an Electrolyte-Gated Transistor. *Nano Lett.* **2017**, *17* (9), 5238−5243.
(21) Wolcott, A.; Doyeux, V.; Nelson, C. A.; Gearba, R.; Lei, K. W.; Yager, K. G.; Dolocan, A. D.; Williams, K.; Nguyen, D.; Zhu, X. Y. Anomalously large polarization effect responsible for excitonic red shifts in PbSe quantum dot solids. *J. Phys. Chem. Lett.* **2011**, *2* (7), 795−800.
(22) Fang, H.; Bechtel, H. A.; Plis, E.; Martin, M. C.; Krishna, S.; Yablonovitch, E.; Javey, A. Quantum of optical absorption in two-dimensional semiconductors. *Proc. Natl. Acad. Sci. U. S. A.* **2013**, *110* (29), 11688−11691.
(23) Oh, S. J.; Berry, N. E.; Choi, J. H.; Gaulding, E. A.; Lin, H.; Paik, T.; Diroll, B. T.; Muramoto, S.; Murray, C. B.; Kagan, C. R. Designing High-Performance PbS and PbSe Nanocrystal Electronic Devices through Stepwise, Post-Synthesis, Colloidal Atomic Layer Deposition. *Nano Lett.* **2014**, *14* (3), 1559−1566.
(24) Araujo, J. J.; Brozek, C. K.; Kroupa, D.; Gamelin, D. R. Degenerately n-Doped Colloidal PbSe Quantum Dots: Band Assignments and Electrostatic Effects. *Nano Lett.* **2018**, *18* (6), 3893−3900.
(25) Boehme, S. C.; Vanmaekelbergh, D.; Evers, W. H.; Siebbeles, L. D. A.; Houtepen, A. J. In Situ Spectroelectrochemical Determination of Energy Levels and Energy Level Offsets in Quantum-Dot Heterojunctions. *J. Phys. Chem. C* **2016**, *120* (9), 5164−5173.
(26) Koh, W. K.; Koposov, A. Y.; Stewart, J. T.; Pal, B. N.; Robel, I.; Pietryga, J. M.; Klimov, V. I. Heavily doped n-type PbSe and PbS nanocrystals using ground-state charge transfer from cobaltocene. *Sci. Rep.* **2013**, *3*, 1−8.
(27) Wehrenberg, B. L.; Guyot-Sionnest, P. Electron and hole injection in PbSe quantum dot films. *J. Am. Chem. Soc.* **2003**, *125* (26), 7806−7807.
(28) Wehrenberg, B. L.; Yu, D.; Ma, J.; Guyot-Sionnest, P. Conduction in charged PbSe nanocrystal films. *J. Phys. Chem. B* **2005**, *109* (43), 20192−20199.
(29) Evers, W. H.; Schins, J. M.; Aerts, M.; Kulkarni, A.; Capiod, P.; Berthe, M.; Grandidier, B.; Delerue, C.; van Der Zant, H. S. J.; van Overbeek, C.; Peters, J. L.; Vanmaekelbergh, D.; Siebbeles, L. D. A.; et al. High charge mobility in two-dimensional percolative networks of PbSe quantum dots connected by atomic bonds. *Nat. Commun.* **2015**, *6*, 1−8.
(30) Kulkarni, A.; Evers, W. H.; Tomić, S.; Beard, M. C.; Vanmaekelbergh, D.; Siebbeles, L. D. A. Efficient Steplike Carrier Multiplication in Percolative Networks of Epitaxially Connected PbSe Nanocrystals. *ACS Nano* **2018**, *12* (1), 378−384.
(31) Kaindl, R. A.; Hägele, D.; Carnahan, M. A.; Chemla, D. S. Transient terahertz spectroscopy of excitons and unbound carriers in quasi-two-dimensional electron-hole gases. *Phys. Rev. B: Condens. Matter Mater. Phys.* **2009**, *79* (4), 1−13.
(32) Ambigapathy, R.; Bar-Joseph, I.; Oberli, D. Y.; Haacke, S.; Brasil, M. J.; Reinhardt, F.; Kapon, E.; Deveaud, B.; et al. Coulomb correlation and band gap renormalization at high carrier densities in quantum wires. *Phys. Rev. Lett.* **1997**, *78* (18), 3579−3582.
(33) Hangleiter, A.; Jin, Z.; Gerhard, M.; Kalincev, D.; Langer, T.; Bremers, H.; Rossow, U.; Koch, M.; Bonn, M.; Turchinovich, D. Efficient formation of excitons in a dense electron-hole plasma at room temperature. *Phys. Rev. B: Condens. Matter Mater. Phys.* **2015**, *92* (24), 1−5.
(34) Lauth, J.; Kulkarni, A.; Spoor, F. C. M.; Renaud, N.; Grozema, F. C.; Houtepen, A. J.; Schins, J. M.; Kinge, S.; Siebbeles, L. D. A. Photogeneration and Mobility of Charge Carriers in Atomically Thin Colloidal InSe Nanosheets Probed by Ultrafast Terahertz Spectroscopy. *J. Phys. Chem. Lett.* **2016**, *7* (20), 4191−4196.
(35) Lauth, J.; Kinge, S.; Siebbeles, L. D. A. Ultrafast Transient Absorption and Terahertz Spectroscopy as Tools to Probe Photo-excited States and Dynamics in Colloidal 2D Nanostructures. *Z. Phys. Chem.* **2017**, *231* (1), 107−119.
(36) Ulbricht, R.; Hendry, E.; Shan, J.; Heinz, T. F.; Bonn, M. Carrier dynamics in semiconductors studied with time-resolved terahertz spectroscopy. *Rev. Mod. Phys.* **2011**, *83* (2), 543−586.
(37) Joyce, H. J.; Boland, J. L.; Davies, C. L.; Baig, S. A.; Johnston, M. B. A review of the electrical properties of semiconductor nanowires: insights gained from terahertz conductivity spectroscopy The influence of surfaces on the transient terahertz conductivity and electron mobility of GaAs nanowires. *Semicond. Sci. Technol.* **2016**, *31*, 103003.

DOI: 10.1021/acs.jpcc.9b03549
J. Phys. Chem. C 2019, 123, 14058−14066

(38) Lloyd-Hughes, J.; Jeon, T. I. A review of the terahertz conductivity of bulk and nano-materials. *J. Infrared, Millimeter, Terahertz Waves* **2012**, *33* (9), 871−925.
(39) Spoor, F. C. M.; Kunneman, L. T.; Evers, W. H.; Renaud, N.; Grozema, F. C.; Houtepen, A. J.; Siebbeles, L. D. A. Hole cooling is much faster than electron cooling in pbse quantum dots. *ACS Nano* **2016**, *10* (1), 695−703.
(40) Spoor, F. C. M.; Tomić, S.; Houtepen, A. J.; Siebbeles, L. D. A. Broadband Cooling Spectra of Hot Electrons and Holes in PbSe Quantum Dots. *ACS Nano* **2017**, *11* (6), 6286−6294.
(41) Smith, N. V. Classical generalization of the Drude formula for the optical conductivity. *Phys. Rev. B: Condens. Matter Mater. Phys.* **2001**, *64* (15), na.
(42) Bergren, M. R.; Kendrick, C. E.; Neale, N. R.; Redwing, J. M.; Collins, R. T.; Furtak, T. E.; Beard, M. C. Ultrafast electrical measurements of isolated silicon nanowires and nanocrystals. *J. Phys. Chem. Lett.* **2014**, *5* (12), 2050−2057.
(43) Beard, M. C.; Turner, G. M.; Murphy, J. E.; Micic, O. I.; Hanna, M. C.; Nozik, A. J.; Schmuttenmaer, C. A. Electronic Coupling in InP Nanoparticle Arrays. *Nano Lett.* **2003**, *3* (12), 1695−1699.
(44) Kittle, C. *Introduction to Solid State Physics*, 7th ed.; Wiley, 2004.
(45) Kang, I.; Wise, F. W. Electronic structure and optical properties of PbS and PbSe quantum dots. *J. Opt. Soc. Am. B* **1997**, *14* (7), 1632.
(46) Liu, Y.; Tolentino, J.; Gibbs, M.; Ihly, R.; Perkins, C. L.; Liu, Y.; Crawford, N.; Hemminger, J. C.; Law, M. PbSe Quantum Dot Field-Effect Transistors with Air-Stable Electron Mobilities above 7 $cm^2 V^{-1} s^{-1}$. *Nano Lett.* **2013**, *13* (4), 1578−1587.
(47) Talgorn, E.; Gao, Y.; Aerts, M.; Kunneman, L. T.; Schins, J. M.; Savenije, T. J.; Van Huis, M. A.; Van Der Zant, H. S. J.; Houtepen, A. J.; Siebbeles, L. D. A. Unity quantum yield of photogenerated charges and band-like transport in quantum-dot solids. *Nat. Nanotechnol.* **2011**, *6* (11), 733−739.
(48) Balazs, D. M.; Matysiak, B. M.; Momand, J.; Shulga, A. G.; Ibáñez, M.; Kovalenko, M. V.; Kooi, B. J.; Loi, M. A. Electron Mobility of 24 $cm^2 V^{-1} s^{-1}$ in PbSe Colloidal-Quantum-Dot Superlattices. *Adv. Mater.* **2018**, *30* (38), 1802265.
(49) Steckel, J. S.; Yen, B. K. H.; Oertel, D. C.; Bawendi, M. G. On the mechanism of lead chalcogenide nanocrystal formation. *J. Am. Chem. Soc.* **2006**, *128* (40), 13032−13033.

DOI: 10.1021/acs.jpcc.9b03549
J. Phys. Chem. C 2019, 123, 14058−14066